# Optimal DC link voltage stabilisation technique for a grid-connected PV system

Taimoor Ahmad Khan[1] , Fadi Kahwash*[1] , Jubaer Ahmed[2] , Keng Goh[1]
[1]*School of Engineering and Mathematics, Edinburgh Napier University, Edinburgh EH10 5DT, United Kingdom*
[2]*School of Computing, Engineering & Built Environment, Edinburgh Napier University, Edinburgh EH10 5DT, United Kingdom*

***Abstract*—The integration and utilisation of renewable energy resources (RES) have seen significant growth due to increased demand and environmental concerns. These RES resources are often integrated through a DC link. The stability and maintaining the DC link voltage at a specific level is of prime importance to ensure smooth and efficient operation in the presence of fluctuating RES. High penetration of these fluctuating resources and load power causes instability at the DC link, which needs to be addressed. A fractional order super twisting sliding mode control technique (FOSTSMC) is proposed in this regard to stabilise the voltage, reduce response time, and overshoot at the DC link of a grid-connected microgrid. The proposed control technique is implemented in a grid-integrated microgrid composed of a photovoltaic (PV) system with an incremental conductance and integral regulator-based maximum power point tracking (IC+IR MPPT) algorithm to extract maximum power. Firstly, a conventional proportional-integral (PI) control-based voltage control technique is implemented, which is considered a benchmark technique for comparison and validation purposes. The results of the benchmark technique exhibit higher overshoot, response time and larger settling time. Secondly, the proposed control technique is implemented to control the DC link voltage to a reference voltage in both constant and varying irradiance. Additionally, to overcome the parameter tuning complexity related to the FOSTSMC, an Ant colony optimisation algorithm is utilised to optimally tune the coefficients of the FOSTSMC controller. The algorithm optimally tunes the parameters of the FOSTSMC to enhance the dynamic stability and overall performance. The simulations are carried out for two cases: with constant irradiance and varying irradiance. The simulation results demonstrated the effectiveness of the ACO-FOSTSMC which exhibits 72% lower settling time, and no overshoot when compared with the benchmark technique. The benchmark technique exhibits longer settling time with a 23.6% overshoot, and 26% undershoot.**

***Index Terms*—FOSTSMC, microgrid, renewable energy, DC voltage control, PID**

## I. Introduction

Amidst the environmental concerns attributed to conventional fuel-based energy generation, RES emerges as a promising solution to fulfil energy needs and curtail carbon emissions simultaneously [1]. Over the past decade, significant advancements have been achieved in the wide adoption of RES resources and their integration into power systems as microgrids [2]. Microgrids are locally controlled and installed to facilitate the main grid in terms of reduced transmission losses, enhanced reliability, advanced monitoring, optimisation capabilities, and multi-operation mode operation. Solar and wind power energies are the most commonly used technology to produce electrical energy, however, the output depends on various climatic conditions and factors. These energy resources are often connected with the DC link using DC-DC boost/buck converters, which are widely adopted for small-scale systems due to their low cost and design simplicity.

Solar energy electrical output depends on meteorological conditions. Therefore, to adjust the power by the load requirements, various traditional and intelligent algorithms for MPPT are proposed, which are based on perturbation and observation algorithms, fuzzy logic, artificial neural networks, model predictive control, heuristic algorithms and incremental conductance algorithms [3]. The effectiveness of these algorithms for MPPT applications is mostly validated using experimental setup, however, high complexity and computational and slow convergence are some of the barriers to wide adoption for real projects. The primary hurdle in integrating RES into a microgrid lies in developing suitable and robust control techniques to guarantee stability, control, and effective power management [4]. Various linear control techniques and controllers exhibit limitations in their performance and response to reject system disturbances, achieve robust response, and are typically developed to meet specific operational requirements [5]. The major challenge faced by the utilisation of DC link is the voltage stability and power delivery during high penetration RES resources. For instance, non-linear control techniques based on PID controllers are proposed to stabilise the voltage at the DC bus bar. Hu et. al. [6] proposed a coordinated control mechanism based on model predictive control and PI controller to control the power and voltage transfer in a 3.5MW AC and DC grid. Similar works are proposed in the literature, where Benlahbib et. al. [7] proposed fractional order PID for DC link voltage regulation in a RES-based hybrid system. Ibrahim et. al. [8] proposed a PID control technique for a similar purpose for an AC microgrid. Nanyan et. al. [9] proposed an optimal PID controller using a sine cosine algorithm for a DC-DC buck converter for a microgrid. Kotra and Mishra [10] carried out a study conducting design and stability analysis of a DC microgrid composed of battery supercapacitor-based storage systems using a PI controller. The majority of these studies adopted conventional PID controller-based techniques which leads to higher settling time and overshoot for voltage stabilisation. Several other techniques to control the voltage are proposed in the literature, which include loop shaping, robust control using Hammerstein identification, and current programmed control techniques [12]. Compared with the conventional control techniques, a

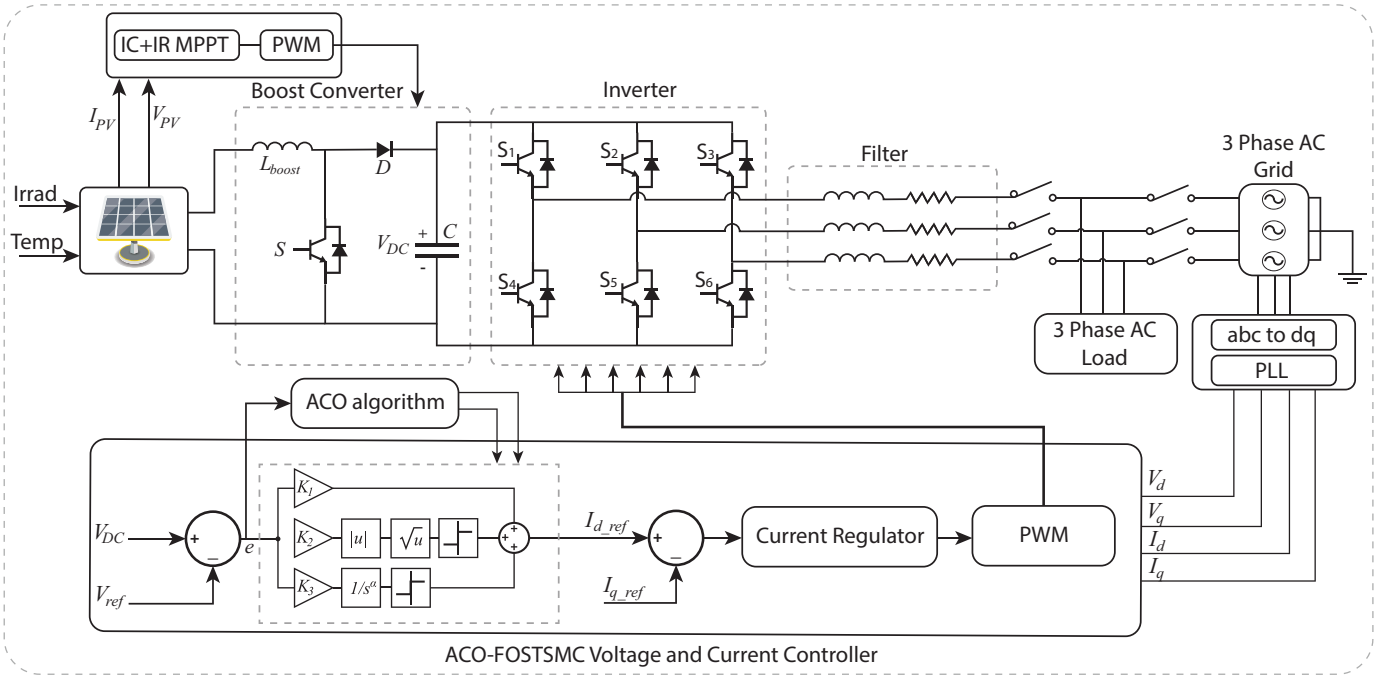


Fig. 1: Proposed control scheme of 3-phase grid-connected PV system

sliding mode controller (SMC) is considered suitable in the literature to mitigate the stabilisation of DC link voltage [13]. SMC possess high robustness and fast response to minimise the error between the reference value and feedback value, however, the response of the system consists of a chattering phenomenon [14]. Several other variants were introduced to resolve and weaken the chattering phenomenon. These variants include terminal SMC (TSMC), second order SMC (SOSMC), adaptive SMC (ASMC), STSMC, etc. which tend to resolve the chattering phenomenon and improve the robustness of the system and were found effective [15]. These variants can be found effective in controlling the voltage source inverter and stabilising the DC link voltage. However, the SMC controller suffers from a parameter tuning issue with lengthy parametric adjustments to exhibit robust response. In this context, several research works focused on tuning mechanisms for PID controllers using ACO algorithm [16]. Several other recent research works proposed ACO-based tuning methods for controllers like classical, and sliding mode controllers [17], and [18]. However, in this work, we have utilized the ACO algorithm for the tuning of FOSTSMC parameters, to achieve acceptable response time, settling time, and lesser overshoot with effective voltage stabilisation.

To overcome the challenges related to the DC link voltage regulation and stabilisation for grid-connected PV-based microgrids, this work presents an optimal control strategy based on ACO-FOSTMC controller to stabilise the DC link voltage, reduce overshoot, settling time and steady-state error. An ACO algorithm is utilised to mitigate the tuning challenge related to the FOSTSMC controller to present a robust response. A grid-connected microgrid scenario is developed in MATLAB/Simulink to validate the results using simulations. The control strategy is tested, firstly applying constant irradiance, and then varying irradiance. As a result, the ACO-FOSTSMC improves the DC link stability and effectively reduces overshoot and settling time. The rest of this work is organized as follows. Section II presents overall grid-connected microgrid modelling and architecture, proposed ACO-based FOSTSMC control strategy and controller development. In Section III, the simulation results for our proposed technique and benchmark control strategy are discussed. Finally, Section IV concludes the paper.

## II. System Configuration and Architecture

The microgrid considered in the current study involves controlling of boost converter along with a maximum power extraction algorithm based on incremental conductance and an integral regulator-based MPPT algorithm for PV systems. The algorithm is aimed at extracting maximum power from the PV while also stabilising the voltage at the DC link improving settling time, overshoot etc. A FOSTSMC along with an ACO controller is proposed to stabilise the voltage DC link.

### A. Grid connected microgrid modelling

The overall modelling of the system is carried out in MATLAB/Simulink, where the ACO algorithm is developed in MATLAB, and grid-connected microgrid modelling is carried out in Simulink. A block diagram showing the overall scenario developed in MATLAB/Simulink is illustrated in Fig. 1. The PV system's characteristics are shown in Table I. The output current of the PV model can be calculated using a nonlinear mathematical exponential expression using Eq. (1 - 3) mentioned in [19].

$$I_{PV} = I_{PH} - I_{SAT1}\left[\exp\left(\frac{V_D}{a_1 V_T}\right) - 1\right] - P_2 \qquad (1)$$

TABLE I: PV specifications of Victron solar panel 90W-12V

| Parameters | Values |
|---|---|
| Nominal Power | 90W |
| No. cells in series | 36 |
| Open circuit voltage ($V_{OC}$) | 23.44 V |
| Short circuit current $I_{SC}$ | 4.61 A |
| Voltage at MPP | 19.5 |
| Temperature coefficient of $V_{OC}$ | -0.35 (%/deg.C) |
| Temperature coefficient of $I_{SC}$ | 36 |
| Parallel strings | 2 |
| Series connected modules per string | 6 |
| Total power at MPP | 1078.74 W |

$$P_2 = I_{SAT2}\left[\exp\left(\frac{V_D}{a_2 V_T}\right) - 1\right] - \frac{(V_{PV} + I_{PV}R_S)}{R_{SH}} \quad (2)$$

$$I_{PH} = [I_{PH-STC} + K_S(T_C - T_{STC})] \times \left(\frac{G}{G_{STC}}\right) \quad (3)$$

Where, $I_{PV}$, $I_{PH}$, $I_{SAT}$, $V_D$, $a$, $V_T$, $T_C$, G, and $G_{STC}$, represents PV output current, photocurrent, reverse saturation current, diode voltage, diode ideal constant, diode thermal voltage, ambient temperature, and standard test condition temperature. Along with the PV array, a boost converter is designed to step up the DC voltage of the PV to convert it into an AC voltage [19].

The boost converter is followed by a grid-connected inverter, which performs grid synchronisation, and monitoring of power flow using pulse width modulation. A voltage source and current source control inverter topology is adopted to design the inverter using size IGBT switches for the current system model, which is shown mathematically using Eq. (4, 5), and is calculated based on the conversion of voltage from natural to synchronous (d-q) reference frame.

$$\begin{bmatrix} v_d \\ v_q \end{bmatrix} = \sqrt{\frac{2}{3}} \begin{bmatrix} \sin\omega\tau & \sin(\omega\tau - 2\pi/3) & \sin(\omega\tau + 2\pi/3) \\ \cos\omega\tau & \cos(\omega\tau - 2\pi/3) & \cos(\omega\tau + 2\pi/3) \end{bmatrix} \quad (4)$$

$$\begin{bmatrix} i_d \\ i_q \end{bmatrix} = \sqrt{\frac{2}{3}} \begin{bmatrix} \sin\omega\tau & \sin(\omega\tau - 2\pi/3) & \sin(\omega\tau + 2\pi/3) \\ \cos\omega\tau & \cos(\omega\tau - 2\pi/3) & \cos(\omega\tau + 2\pi/3) \end{bmatrix} \quad (5)$$

### *B. ACO-FOSTMC*

Fractional order calculus involves both the integration and differentiation with an additional fractional order operator known as $D_t^r$ and represented using Eq. 6. The FOSTSMC controller has 4 coefficients: K1, K2, K3 and fractional operator. K1 can be referred to as the proportional control coefficient, K2 is in the range [0 1] and is used to reduce the chattering effect in the response of the system, while K3 can be referred to as the integral control coefficient.

$$\alpha D_t^r = \begin{cases} {}^{d^r}/_{dt^r} & \alpha > 0 \\ 1 & \alpha = 0 \\ \int_\alpha^t (dt)^r & \alpha < 0 \end{cases} \quad (6)$$

Peng et. al. [20] presented a Grunwald-Letnikov-based approximate definition for the fractional integrodifferential mathematically represented in Eq. 7. Where, $\begin{pmatrix} r \\ j \end{pmatrix}$ is the binomial coefficient, "$\alpha$" and "t" are the lower and upper integration limits, and the values of these depend on the integral and differentiation. Reimann-Liuoville also gave another definition to represent the fractional integro-differential, which is shown using Eq. 8.

$$\alpha D_t^r = \lim_{h\to 0} h^{-1} \sum_{j=0} (-1)^j \begin{pmatrix} r \\ j \end{pmatrix} f(t - jh) \quad (7)$$

$$\alpha D_t^r f(t) = \frac{1}{(n-r)} \left(\frac{d}{dt}\right)^n \int_\alpha^t \frac{f(\tau)}{(t-\tau)^{r-n+1}} d\tau \quad (8)$$

A simplified version of the fractional approximation algorithm using the recursive distribution of the poles and zeroes which is shown using Eq. (9) [21]. Where, K, M, $w_{z,n}$, $w_{p,n}$, $w_t$, and $w_h$ represents gain of function, no. of poles and zeroes, frequency of poles, frequency of zeroes, lower frequency and high frequency, which can be calculated using Eqs. (10 - 13).

$$s^\alpha = K \prod_{m=1}^{M} \frac{1 + (s/w_{z,n})}{1 + (s/w_{z,n})}, \alpha > 0 \quad (9)$$

$$w_{z,1} = w_l\sqrt{\eta} \quad (10)$$

$$w_{p,n} = w_{z,n}\xi \quad (11)$$

$$w_{z,n+1} = w_{p,n}, \eta \quad (12)$$

$$\xi = \left(\frac{w_h}{w_l}\right)^{\left(\frac{1-\alpha}{M}\right)} \quad (13)$$

$$C(s) = K_1(e) + K_2(\sqrt{|e|})sign(e) + v \quad (14)$$

$$v = (K_3 D_t^\alpha)sign(e) \quad (15)$$

Furthermore, to tune the parameters of the FOSTSMC mentioned in Eq. (14 - 16), the ACO algorithm is utilised to optimally tune these parameters. The objective function for the ACO algorithm is mathematically represented using Eq. 16.

$$f(obj) = ITAE(IntegralSquareError) = \int_0^\infty t|e(t)|dt \quad (16)$$

The reference voltage and closed loop feedback are considered for the evaluation of the objective function for the optimization problem to search for the optimal combination. Initially, only one cost function is considered, after which the best nodes identified are then considered for the single objective function. In the trip of food search, the ants cross the joints and choose from a track among "Ns" and "Nd" nodes, where the main objective is considered. To find out the optimal journey with minimized cost in the FOSTSMC function. To choose the nodes "i" to "j" a rule of probability for the $K_{th}$ and $A_{ij}^k$ is given in Eq. 17.

$$A_{ij}^{k} = \left\{ \begin{array}{ll} \frac{\left[\gamma_{ij}^{\alpha}\right]\left[\eta_{ij}^{\beta}(n)\right]}{\sum c_{il} \in N(S^P)\left[\tau_{ij}^{\alpha}(n)\right]\left[\eta_{ij}^{\beta}(n)\right]} & if\ c_{il} \in N\left(S^P\right) \\ 0 & otherwise \end{array} \right\} \quad (17)$$

In Eq. 17, the partial solution can be represented by $S^P$, whereas the possible nodes' set of ants is represented by $N(S^P)$, the possible path not visited by the ant "K" can be represented by "l", the intensity of spice between nodes "i" and "j" can also be represented by $\gamma_{ij}^{k}$, and heuristic intensity between the nodes "i" and "j" is shown by $\eta_{ij}^{k}$.

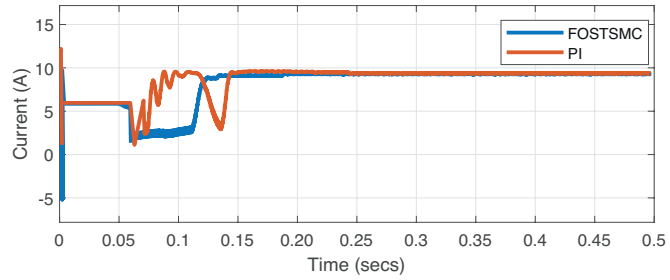


(a) PV current with PI and ACO-FOSTSMC

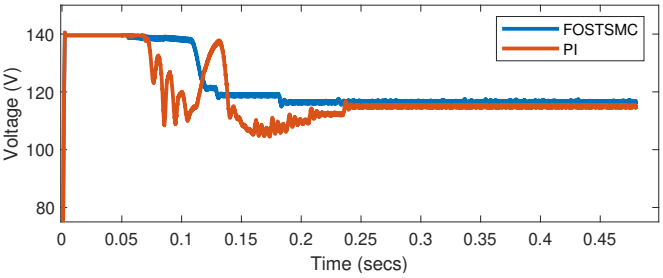


(b) PV voltage with PI and ACO-FOSTSMC

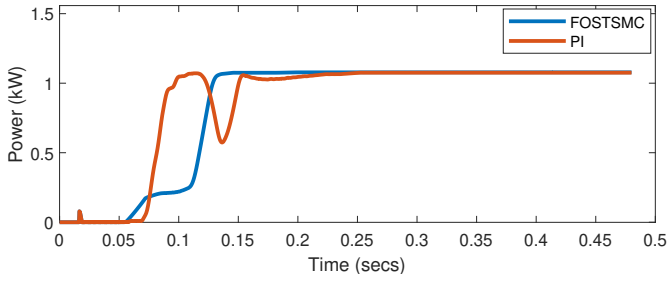


(c) PV Power with PI and ACO-FOSTSMC

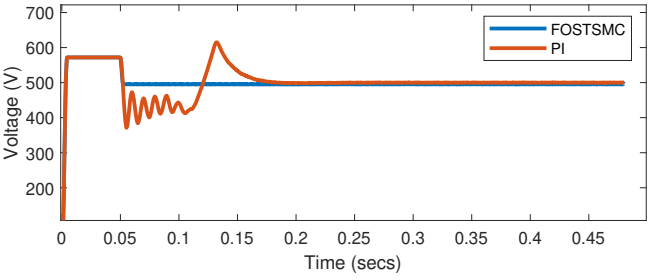


(d) DC Link voltage with PI and ACO-FOSTSMC

Fig. 2: Simulation results for the proposed control strategy with a constant irradiance 1000 $W/m^2$ at $25^oC$.

$$\gamma_{ij}(n)^{worst} = \gamma_{ij}(n)^{worst} - \left(\frac{0.3 \times a}{C_{worst}}\right) \quad (18)$$

$$\gamma_{ij}(n)^{best} = \gamma_{ij}(n)^{best} + \left(\frac{a}{C_{best}}\right) \quad (19)$$

$$\gamma_{ij}^{k} = \gamma_{ij}^{k}(n-1) + \left(\frac{0.2 \times a}{C}\right) \quad (20)$$

The trail and analytical information values are represented by the $\alpha$ and $\beta$ respectively, whereas the ant spice values are updated by negative update rules, global spice positive, and local spice according to Eq. 18, Eq. 19, and Eq. 20. Whereas, the general spice renovating factor is termed as a minimal function of the overall trip and can be represented by "C" of an ant "k".

## III. Simulations Results Analysis

The performance of the system model using the proposed control strategy for the DC link voltage regulation is carried out using MATLAB/Simulink. The overall 3-phase grid-connected PV-powered microgrid is developed in Simulink, whereas the optimisation algorithm utilised for the optimised coefficient tuning is carried out in MATLAB as illustrated in Fig. 1. An incremental conductance and integral regulator-based MPPT algorithm [22] is utilised with the proposed control strategy to maximise the PV output. To validate the performance of the proposed system model, firstly a constant 1000 $W/m^2$ irradiance at $25^oC$ is applied to the PV system. Secondly, a variable irradiance with sharp decrease and increase is also applied to evaluate the performance of the proposed control strategy in varying weather conditions. In the first case, with a constant irradiance, the results are shown in Fig. (2), which shows the PV voltage, current, power and DC link voltage. Fig. (2a), shows the PV current using the proposed ACO-FOSTSMC strategy and PI controller, a large overshoot and longer settling time can be observed in the PI result for current, whereas the ACO-FOSTSMC having comparatively lesser overshoot and fast settling time. Similarly, Fig. (2b) shows the PV voltage for the constant irradiance, which also possesses overshoot and longer settling time as compared with the ACO-STSMC. Fig. (2c) depicts the PV power with IC+IR MPPT. The power output having a PI controller, starts with a sharp increase at 0.07 secs, however drops sharply again at 0.12 secs and settles again at 0.2 secs. However, the ACO-STSMC started tracing at 0.13 secs without any overshoot at the start. From Fig. (2d) it can be observed the PI controller-based strategy exhibits a large undershoot and longer settling time whereas stabilises after 0.17secs. Concurrently, the proposed ACO-FOSTSMC-based strategy stabilises the DC link voltage directly after starting the simulations at 0.05 secs without an overshoot at the start. To evaluate the performance of our proposed strategy, varying irradiance is applied to the system model consisting of sharp increase and decrease. The results are shown in Fig. (3), which shows the irradiance, PV current, voltage, power and DC link voltage. A total of 11 points of varying irradiance are applied between 0 and 2.2 secs, as depicted in Fig. (3a).

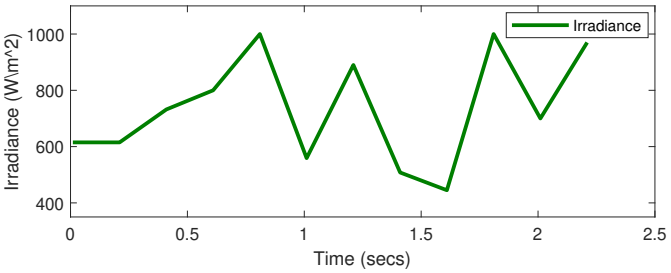


(a) Irradiance

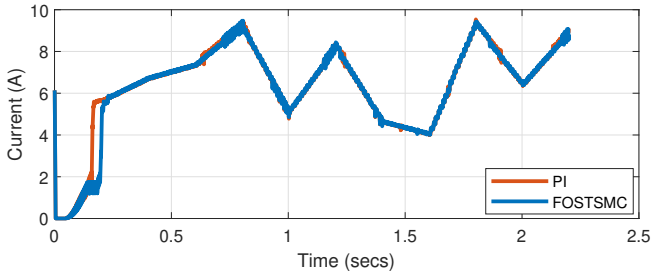


(b) PV current with PI and ACO-FOSTSMC

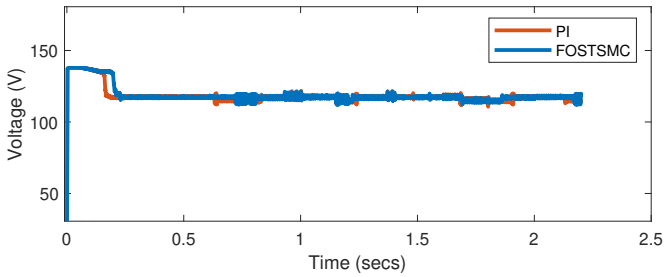


(c) PV voltage with PI and ACO-FOSTSMC

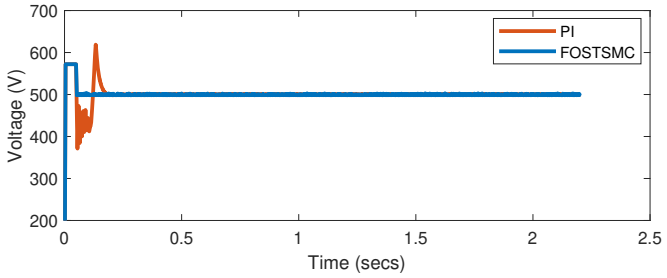


(d) PV Power with PI and ACO-FOSTSMC

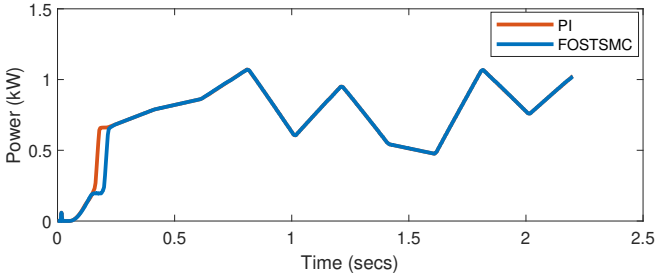


(e) PV Power with PI and ACO-FOSTSMC

Fig. 3: Simulation results with varying irradiance using PI and FOSTMC.

The current and voltage waveforms of the PV for the PI and ACOFOSTSMC are shown in Fig. (3b) and Fig. (3c) respectively. Due to the smooth increase in the irradiance at the start, the PI controller did not overshoot as it did in the case of constant irradiance. However, in the case of the DC link voltage stabilisation, a clear overshoot and undershoot can be observed in Fig. (3d). PI control-based strategy started tracing the DC ref voltage at 0.2 secs, and the ACO-FOSTSMC-based control strategy started tracing at 0.05 secs. The overshoot here is due to the MPPT and VSC controller settling delay, which is introduced using a step input signal at 0.05 for both the constant and varying irradiance cases.

After the completion of the simulation for both cases, the results demonstrate that the ACO-STSMC outperforms the PI-based strategy in terms of overshoot and settling time. For the case of constant irradiance, the ACO-FOSTSMC settling time is up to 50% lesser when compared with the PI control-based strategy. Similarly, for the case of PV voltage, the settling time is also 50% lesser, and vice versa for the case of PV power with a high undershoot in the case of PI control-based strategy. The DC link voltage is stabilised more effectively using the proposed system model with almost no overshoot, lesser settling time and steady-state error. The settling time for the FOSTSMC is 72.2% lower than the benchmark PI-based control strategy.

## IV. Conclusion

This paper proposes a DC link voltage regulation and stabilisation strategy based on the ACO-FOSTSMC control technique for a grid-connected PV system. An IC+IR MPPT algorithm is also utilised with the PV system to extract maximum power, which is then connected with a grid using a 3-level inverter supplying 3-phase power to the load. The FOSTSMC control technique is deployed to stabilise the voltage and reduce overshoot, settling time, and steady-state error. A PI controller-based benchmark strategy, which is widely adopted, is also deployed to validate the results of our proposed technique. The simulation results are carried out for two cases of irradiance using constant and varying values over time. The simulation results suggest that the proposed technique exhibits better results when compared with the benchmark technique with no overshoot, steady-state error and lesser settling time when compared with the PI control-based strategy.

## References

[1] Y. R. O, J. J, A. K. Chakraborty, and J. M. Guerrero, "Stability Constrained Optimal Operation of Standalone DC Microgrids Considering Load and Solar PV Uncertainties," IEEE Transactions on Power Delivery, vol. 38, no. 4, pp. 2673-2681, 2023, doi: 10.1109/tpwrd.2023.3253623.

[2] B. Modu, M. P. Abdullah, M. A. Sanusi, and M. F. Hamza, "DC-based microgrid: Topologies, control schemes, and implementations," Alexandria Engineering Journal, vol. 70, pp. 61-92, 2023, doi: 10.1016/j.aej.2023.02.021.

[3] M. H. Ibrahim, S. P. Ang, M. N. Dani, M. I. Rahman, R. Petra, and S. M. Sulthan, "Optimizing Step-Size of Perturb & Observe and Incremental Conductance MPPT Techniques Using PSO for Grid-Tied PV System," IEEE Access, vol. 11, pp. 13079-13090, 2023.

[4] S. Kundu, M. Singh, and A. K. Giri, "Synchronization and control of WECS-SPV-BSS-based distributed generation system using ICCF-PLL control approach," Electric Power Systems Research, vol. 226, p. 109919, 2024.

[5] C. Lakhdairi, A. Benaboud, H. Bahri, and M. Talea, "A Review Study of Control Strategies of VSC-HVDC System Used Between Renewable Energy Source and Grid," in International Conference on Digital Technologies and Applications, 2023: Springer, pp. 664-673.
[6] J. Hu, Y. Shan, Y. Xu, and J. M. Guerrero, "A coordinated control of hybrid ac/dc microgrids with PV-wind-battery under variable generation and load conditions," International Journal of Electrical Power & Energy Systems, vol. 104, pp. 583-592, 2019, doi: 10.1016/j.ijepes.2018.07.037.
[7] B. Benlahbib, F. Bouchafaa, N. Bouarroudj, and S. Mekhilef, "Fractional order PID controller for DC link voltage regulation in hybrid system including wind turbine- and battery packs-experimental validation," International Journal of Power Electronics, vol. 10, no. 3, pp. 289-313, 2019/01/01 2019, doi: 10.1504/IJPELEC.2019.099346.
[8] I. Alhamrouni, M. Hairullah, N. Omar, M. Salem, A. Jusoh, and T. Sutikno, "Modelling and design of PID controller for voltage control of AC hybrid micro-grid," International Journal of Power Electronics and Drive Systems, vol. 10, no. 1, p. 151, 2019.
[9] N. F. Nanyan, M. A. Ahmad, and B. Hekimoğlu, "Optimal PID controller for the DC-DC buck converter using the improved sine cosine algorithm," Results in Control and Optimization, vol. 14, p. 100352, 2024/03/01/ 2024, doi: https://doi.org/10.1016/j.rico.2023.100352.
[10] T. Thomas, M. K. Mishra, C. Kumar, and M. Liserre, "Control of a PV-Wind Based DC Microgrid with Hybrid Energy Storage System Using Lyapunov Approach and Sliding Mode Control," IEEE Transactions on Industry Applications, pp. 1-12, 2024, doi: 10.1109/TIA.2023.3349359.
[11] F. Alonge, R. Rabbeni, M. Pucci, and G. Vitale, "Identification and robust control of a quadratic DC/DC boost converter by Hammerstein model," 2014 IEEE Energy Conversion Congress and Exposition (ECCE), pp. 3355-3362, 2014.
[12] F. S. Al-Ismail, "DC microgrid planning, operation, and control: A comprehensive review," IEEE Access, vol. 9, pp. 36154-36172, 2021.
[13] S. Liu et al., "Application of an Improved STSMC Method to the Bidirectional DC–DC Converter in Photovoltaic DC Microgrid," Energies, vol. 15, no. 5, 2022, doi: 10.3390/en15051636.
[14] M. A. Sharaf et al., "Hybrid Control of the DC Microgrid Using Deep Neural Networks and Global Terminal Sliding Mode Control with the Exponential Reaching Law," Sensors (Basel), vol. 23, no. 23, Nov 22 2023, doi: 10.3390/s23239342.
[15] E. Martinez-Vera and P. Banuelos-Sanchez, "Review of Bidirectional DC-DC Converters and Trends in Control Techniques for Applications in Electric Vehicles," IEEE Latin America Transactions, vol. 22, no. 2, pp. 144-155, 2024.
[16] Ünal, Muhammet, Ayça Ak, Vedat Topuz, and Hasan Erdal. Optimization of PID controllers using ant colony and genetic algorithms. Vol. 449. Springer, 2012.
[17] Ganthia, Bibhu Prasad, Rosalin Pradhan, Rajashree Sahu, and Aditya Kumar Pati. "Artificial ant colony optimized direct torque control of mathematically modeled induction motor drive using pi and sliding mode controller." In Recent Advances in Power Electronics and Drives, pp. 389-408. Springer, Singapore, 2021.
[18] Espin, Jorge, Sebastian Estrada, Diego Benítez, and Oscar Camacho. "Comparison of Bioinspired Optimization Techniques for Improving the Performance of Dynamic Sliding Mode Controllers." In 2022 IEEE Colombian Conference on Applications of Computational Intelligence (ColCACI), pp. 1-6. IEEE, 2022.
[19] Aloo, Linus A., Peter K. Kihato, Stanley I. Kamau, and Roy S. Orenge. "Modeling and control of a photovoltaic-wind hybrid microgrid system using GA-ANFIS." Heliyon 9, no. 4 (2023).
[20] Peng, Yuexi, Jun Liu, Shaobo He, and Kehui Sun. "Discrete fracmemristor-based chaotic map by Grunwald–Letnikov difference and its circuit implementation." Chaos, Solitons & Fractals 171 (2023): 113429.
[21] Yongzhi, L. I. U., L. I. Jie, D. A. I. Cong, and S. H. A. N. Chenglong. "Design of simplified fractional-order PID controller based on improved Oustaloup filter." Information and Control 48, no. 6 (2019): 723-728.
[22] Giroux, Pierre, Olivier Tremblay, Gilbert Sybille, and Patrice Brunelle. "Microgrid dynamic operation." (2021).